SIMULATION OF STRESS DISTRIBUTION IN THE WELD OF A DISSIMILAR JOINT

Aleksander Gwiazda[1], Santina Topolska[2]

[,1] Silesian University of Technology, Faculty of Mechanical Engineering, Department of Engineering Processes Automation and Integrated Manufacturing Systems, Konarskiego 18A, 44-100 Gliwice, Poland
[2] Silesian University of Technology, Faculty of Mechanical Engineering, Department of Welding, Konarskiego 18A, 44-100 Gliwice, Poland

Corresponding author: Aleksander Gwiazda, aleksander.gwiazda@polsl.pl

Abstract: The article presents the investigations of corrosion properties of welded heterogenous joints. These joints were made of duplex steel of grade 2205- X2CrNiMoCuN22-5-3 (1.4462) and of austenitic steel of grade 316L - X2CrNiMo17-12-2 (1.4404). The joint was manufactured using the welding wire P5 (Avesta, Sweden). The aim of the research was to analyze the matching of a numerical model of the joint with the results obtained in the case of an actual one. The paper presents the modellling process of a joint using an advanced CAD / CAE class system. The advantage of utilization the CAE class system is its ability to investigate the behavior of the whole joint in virtual environment. They also allow conducting numerical experiments taking into consideration the dynamical excitations which affect the operation of the analysed construction. The results show that modeling behavior of heterogenous joints in CAE class system basing on experimentally designated material parameters, allow obtaining results more corresponding to reality.
Key words: Welded joints, duplex steels, simulation

1. INTRODUCTION

Duplex steels are stainless steels with a two-phase structure consisting of ferrite with the addition of 40 to 60% austenite. They are also referred as belonging to the family of austenitic-ferritic steels. Their solidification takes place first in the ferritic structure (delta ferrite) followed by a partial conversion in the solid phase to the austenitic structure, therefore some (especially in the welding world) prefer the term ferrite-austenitic (Knyazeva and Pohl, 2013).
Duplex stainless steels include various grades classified according to their chemical composition. This chemical composition based on the high content of chromium, nickel and molybdenum improves the resistance to intercrystalline and pitting corrosion. The presence of two phases of the microstructure guarantees greater resistance to pitting and corrosion cracking compared to conventional stainless steels. The first generation of these steel grades was based on chromium, nickel and molybdenum alloys. Despite their good corrosion resistance properties, welding has resulted in a decrease in their ductility (elasticity) due to the massive presence of a ferritic microstructure, which has limited their use to a few specific applications. The new grades are characterized by the addition of nitrogen as an additive improving the ductility of the welded joint and increasing the resistance to corrosion caused by chlorine. This nitrogen addition promotes structural hardening due to a fine interstitial dispersion mechanism that increases yield point and tensile strength without compromising toughness (Gunn, 2008).
The 2202 grade is the basic duplex steel. Its structure is formed by the aggregate of the ferrite phase (α) and the austenite phase (γ). The two-phase structure of the alloy allows achieving high yield strengths while maintaining good ductility (Gardi, 2006). In fact, hardening is achieved by the ferritic phase, while the austenitic matrix allows ductility and strength to be retained. The mixed structure gives 2202 a high resistance to stress corrosion cracking and makes it insensitive to intergranular corrosion. Continuous use of 2202 at temperatures above 300°C is not recommended for the following reasons: between 350 and 550 ° C: loss of ductility by ferrite brittleness due to the formation of the so-called α 'phase, which may be accompanied by other precipitation from hardening, classic phenomenon of ferritic steels stainless steel, more commonly referred to as brittleness at 475°C (Jebaraja et al., 2017).

2. WELDABILITY OF DUPLEX STEELS

The high temperatures achieved and the high cooling rates encountered in traditional welding processes (Adamiak et al., 2018) will tend to freeze the formed structures of the molten metal and parent metal near the melting line (Chaudhari et al., 2019). An uncontrolled thermal cycle will thus result in incomplete ferrite / austenite conversion, resulting in

a higher ferrite rate than in the base material as delivered (Tahchieva et al., 2019).
The structures obtained in the heat-affected zone (HAZ) as well as in the fusion zone (PZ) and especially in the molten zone (MZ) tend to lose the properties obtained in the as delivered condition. Moreover, the tensile strength will be the lower the higher the ferrite content will be (Rosso et al., 2013).
In order to maintain good mechanical properties and corrosion resistance in the welded joint (Zappa et al., 2013) the following conditions are necessary:

- to select a filler product containing the appropriate gamma elements (promoting the production of austenite), including nitrogen, which can be added to the shielding gas in inert gas welding processes (TIG, MIG, plasma),
- to find a trade-off between the welding energy high enough to necessarily allow a slow cooling to produce 40 to 60% austenitic structure, and low enough to avoid the formation of precipitates such as sigma phases (FeCr), carbides (Cr23C6) or nitrides (Cr2N and CrN),
- when ferrite is present, care should be taken to use low hydrogen fillers to avoid cold cracking and low carbon problems to avoid the formation of chromium carbides which can lead to intergranular corrosion problems.

3. RESEARCH METHODOLOGY

3.1. Specimens description

Two construction materials commonly used in industrial practice were selected as the test material, namely 2205 duplex steel and 316L austenitic steel. Taking into account also the sheet thicknesses that are typical for the industry, a decision was made to use a sheet with a thickness of 15 mm, which thickness allows the preparation of samples for testing in a fairly easy way. Connected elements were cut from larger sheets of metal. Welding process was performed using the 3.2 mm AVESTA P5 welding wire (The Avesta Welding Manual). The chemical composition of these materials is presented in Table 1.

Table 1. Chemical composition of welded materials (%), [on the basis of delivery certificates]

	C	Si	Mn	Cr	Ni	Mo	N
2205	0.027	0.41	0.80	22.8	5.33	3.11	0.16
316L	0.041	0.52	1.69	17.2	9.90	2.10	0.04
AVESTA P5 S 23 12 2 L	0.009	0.32	1.4	21.2	15.1	2.62	0.06

Welding was performed using the automatic submerged arc welding (SAW) technology. It is a very efficient technology.

In the case of duplex steel grade 2205 (in accordance with PN-EN 10088-2: steel grade X2CrNiMoCuN22-5-3, number 1.4462), certified sheets produced by the well-known Finnish concern Outokumpu were used. The used sheets were delivered supersaturated. The supersaturation was carried out at a temperature of 1100°C. Below (Table 1) a comparison of the standard chemical composition of this steel grade, composition according to the certificate and composition according to the spectral analysis performed is presented.
The butt joint was selected for the tests as it is characterized by a more complex state of stress and allows for a more direct assessment of the phenomena affecting the properties of the entire welded joint. For the purpose of the research, four types of butt joint were selected as technical variables of the analyzed process. The face connectors selected were:

- parallel weld, performed without beveling the edges (weld I) with a distance of 1 mm, double-sided, double-pass welding (type 1) is assumed,
- a Y-joint with the edges of the plates beveled at an angle of 30^o (groove throat with an opening angle of 60^o, joint groove depth 11 mm, groove threshold 4 mm, groove distance 1 mm), one-side, multi-pass welding (type 2A) is assumed,
- Y-joint with board edges beveled at 30^o (groove throat with an opening angle of 60^o, weld groove depth 11 mm, groove threshold 4 mm, groove distance 1 mm), one-sided, multi-pass welding (type 2B) is assumed,
- 2Y weld with the board edges beveled at 45^o (groove throat with 90^o opening angle, weld groove depth 5.5 mm, groove threshold 4 mm, groove spacing 1 mm), double-sided, double-run welding (type 3) was assumed.

The difference between types 2A and 2B is the different welding energy. Values of the heat input, during welding, varied between 1.19 kJ/mm (weld No 2A) to 3.64 kJ/mm (weld No 2B).

3.2. Mechanical properties testing

Two static tests were carried out in the field of mechanical properties tests: tensile and bend tests. Properties that are directly measured using a tensile test are: ultimate tensile strength, breaking strength, maximum elongation and reduction in area. This test is performed on a universal testing machine. This type of machine has two crossheads. The first is adjusted for the length of the specimen and the second is driven to apply tension to the test specimen. Whereas bending testing, called the three-point bending flexural test, provides values for the modulus of elasticity in bending, flexural stress, flexural strain and the flexural stress–strain response of the material. This test is performed on a universal testing machine

(tensile testing machine or tensile tester) with a three-point or four-point bend fixture.

4. TESTING

4.1. Tensile testing

The static tensile tests of the joints were carried out for two samples taken from each performed welded joint (R1, R2). Static tensile tests were performed on the Universal Testing Machine 1195 (Instron, USA) in accordance with PN-EN ISO 6892-1: 2016-09 and PN-EN ISO 4136: 2013-05. It is test in which a sample is subjected to a controlled tension until failure. The choosing of only two types was done because it was the auxiliary tests. These samples were stretched on a testing machine. Samples, prepared on the basis of welding joints obtainen using the SAW technology, after the static tensile testing, are shown in Figure 1. In this Figure are presented exemplar samples chosen from the whole set of samples that are representative for this testing results.

The entirety of the tests covered a total of 8 measurements (four types of joint, two test samples). The obtained test results are presented in Table 2. PM is the parent material, S_0 is the initial cross-sectional area and Fm is the breaking force. It can be seen that the break point was always on the side of the 316L austenitic steel in the area of the parent material. The differences in the measured values of the starting section S_0 were less than 4.4%. On the other hand, the differences, in the specified value of the breaking strength Rm, were in the range of no more than approximately 3.0%.

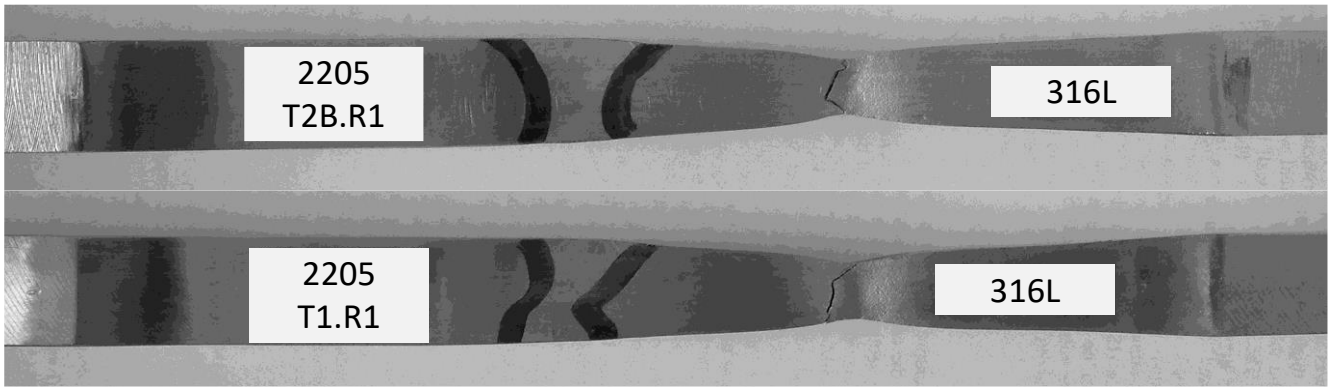

Fig. 1. Samples after the static tensile test, [own elaboration]

Table 2. Results of static tensile tests of welded joints

No	Specimen type	S_0 [mm^2]	F_m [kN]	R_m [MPa]	Fracture placement
1	T1.R1	384.56	230.63	599.72	PM-austenitic steel
2	T1.R2	388.11	226.63	583.93	PM-austenitic steel
3	T2A.R1	372.02	220.49	592.68	PM-austenitic steel
4	T2A.R2	368.59	215.97	585.93	PM-austenitic steel
5	T2B.R1	381.92	227.32	595.20	PM-austenitic steel
6	T2B.R2	384.80	228.63	594.16	PM-austenitic steel
7	T3.R1	383.90	228.14	594.26	PM-austenitic steel
8	T3.R2	384.63	223.93	582.19	PM-austenitic steel

4.2. Bending testing

For the static bending test, two cuboidal test pieces (Z1, Z2) with a cross-section as mentioned 15x25 mm were used from each element. Static bending tests were carried out in accordance with PN-EN ISO 5173: 2010. They were made on the Tensile Testing Machine ZD-40 (WPM, Germany). It was the 3-point technique. The diameter of the bending head was 45 mm, which corresponds to three sheet thicknesses (15 mm). Each sample was bent to an angle of 120°.

Sample Z1 was subjected to stretching bending of the weld face (the weld was placed on the supports from below, the bending head acted on the top of the weld). This case was designated RLS. Sample Z2 was subjected to tensile bending of the weld root (reverse sample positioning) and the RGS was determined. Examples of samples after the static bending test are shown in Figure 2. On the other hand, Table 3 summarizes the results of all the static bending tests performed. As mentioned, a bending head with a diameter of 45 mm was used and the bending was carried out to an angle of 120°. The absence of cracks in all tests allowed determining that all the samples passed the static bending test positively.

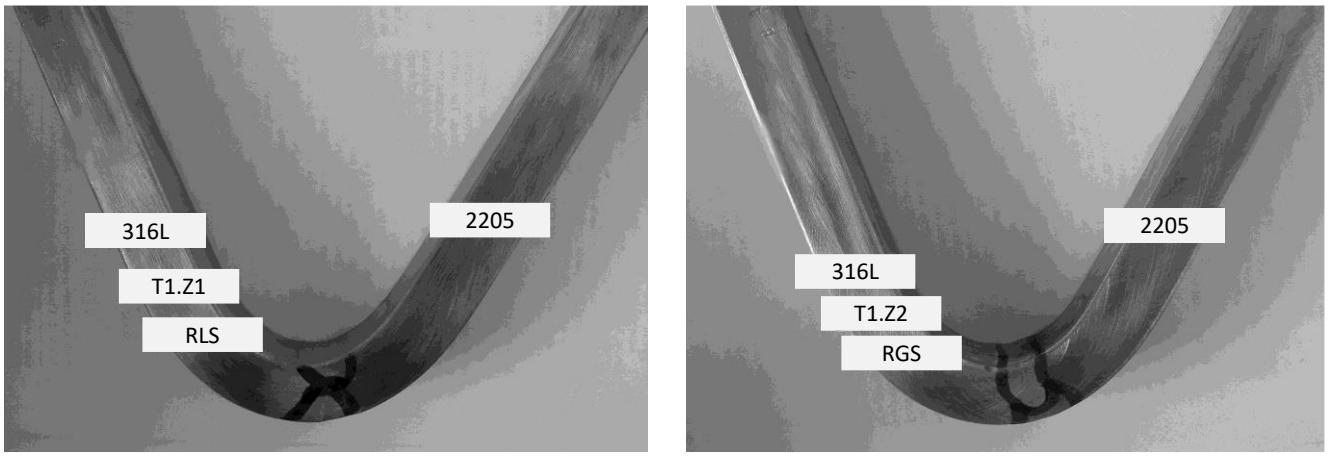

Fig. 2. Exemplary samples after a static bend test, [own elaboration]

Table 3. Results of static bending tests of welded joints

No	Specimen symbol	Bending from the side of	Observation
1	T1.Z1	RLS	no fractures
2	T1.Z2	RGS	no fractures
3	T2A.Z1	RLS	no fractures
4	T2A.Z2	RGS	no fractures
5	T2B.Z1	RLS	no fractures
6	T2B.Z2	RGS	no fractures
7	T3.Z1	RLS	no fractures
8	T3.Z2	RGS	no fractures

5. COMPUTER MODELLING OF TESTING

It has been prepared the two separate models that allow virtually reflect the static testing (Figure 3). For tests the NX PLM (Siemens, Germany) platform was used.

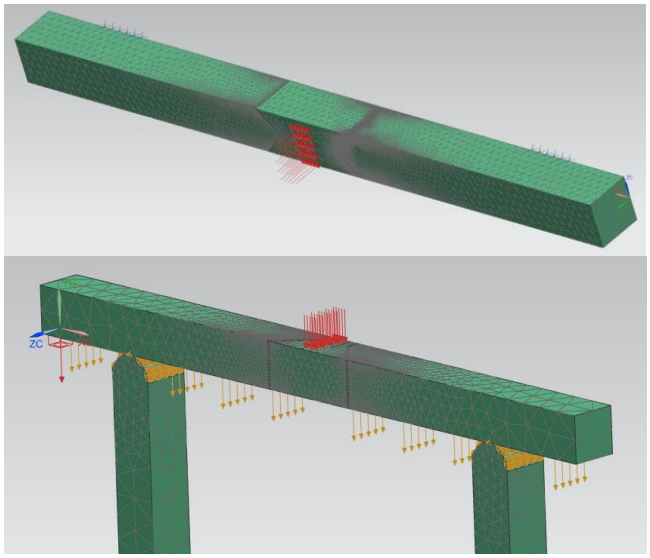
Fig. 3. Virtual models of specimens for virtual testing, [own elaboration]

The aim of this investigation is to determine the procedure of virtual specimen models building. The data obtained in laboratory tests were indtroduced as material parameters of the created model. These models should allow obtaining reasonably well matched information about stresses and strains in the construction of a welded joint.

In Figure 4 is presented the investigated model during conducting the virtual tensile testing. All material characteristics of this virtual model are taken from the material investigations. Introducing the material characteristics let the model be more accurate.

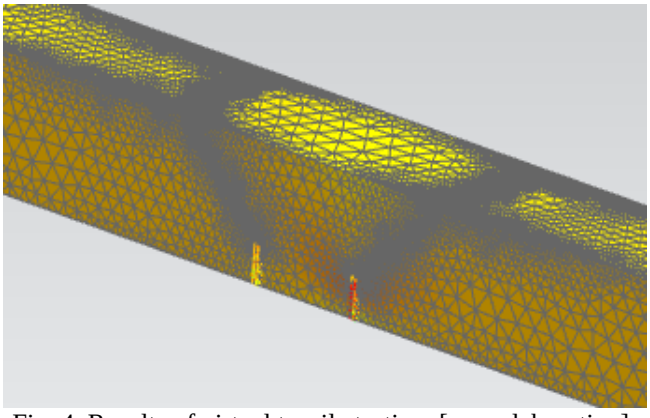
Fig. 4. Results of virtual tensile testing, [own elaboration]

In Figure 5 it could be observed the concentration of stresses in the weld on the side of the 2205 HAZ side, where larger amount of ferrite is observed.

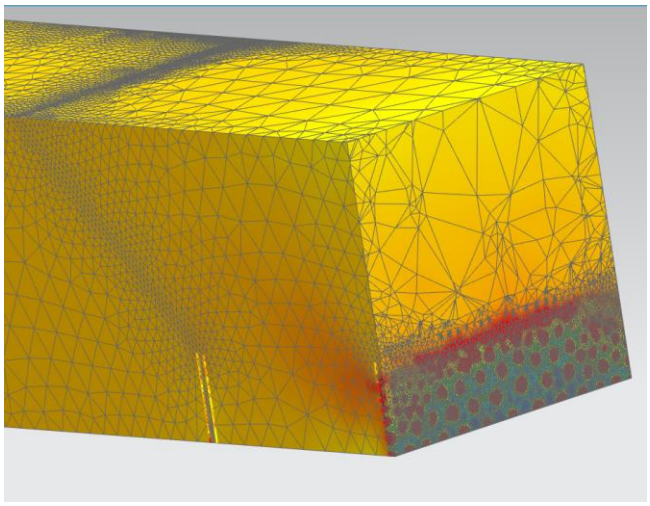

Fig. 5. Results of virtual tensile testing, [own elaboration]

In the same way the virtual method of bending testing was determined. In Figure 6 is presented the results of virtual testing.

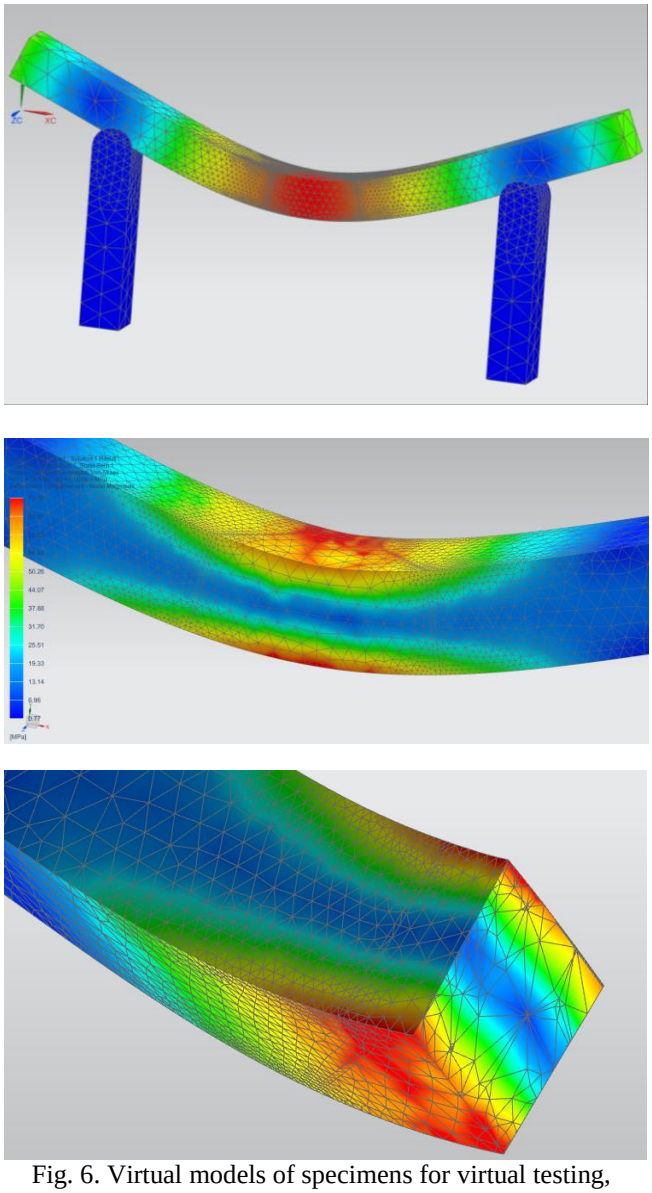

Fig. 6. Virtual models of specimens for virtual testing, [own elaboration]

The obtained results showed the stress concentration during the bending test in the area of the weld root. This result is related to the indicated increase in ferrite content in the cross-section of the weld. In the area of the weld root, the increased content of ferrite results from the effect of multiple thermal energy emission associated with multi-pass welding.

6. CONCLUSIONS

I should be started with some conclusions relating the present study. Mechanical testing regarding strength characteristics show accurate properties of analyzed parameters of joints. More precisely the mechanical properties of the tested welds generally confirm the good mechanical parameters of the resulting welded joints. The average tensile strength R_m of the joint in the static tensile test is 591 MPa. The difference in the results for the tested joints is less than 6.5%. The joints also meet the conditions of a static bend test. This confirms the good mechanical properties of analyzed type of joints at normal conditions (without a corrosion agent influence). The highest average mechanical properties are stated for the joint number 1. The worst for the joint number 2. Other joints are characterized by mechanical properties at middle level.

The models were prepared using material characteristics obtained in laboratory tests. The preparation and analysis of the virtual testing show that the observed stress concentration matches the observation made upon the results of the laboratory testing. Moreover, it is possible to observe the structure of the stresses concentration what is not always possible in laboratory tests, for example in the case of the bending test. So it is possible to determine the security range of elements being bending more precisely that during test conducted according proper standard.

7. REFERENCES

1. Adamiak, M., Czupryński, A., Kopyść, A., Monica, Z., Olender, M., Gwiazda, A., (2018). *The Properties of Arc-Sprayed Aluminum Coatings on Armor-Grade Steel*, Metals, 8/2, 1-10.
2. Chaudhari A. N., Dixit K., Bhatia G. S., Singh B., Singhal P., Saxena K. K., (2019). *Welding Behaviour of Duplex Stainless Steel AISI 2205: A Review*, Materials today: Proceedings, **18**(7), 2731-2737.
3. Gardi R. H., (2006). *Effect of artificial aging time and temperature on tensile strength of duplex stainless steels saf 2205 and saf 2304 using (abi) technique*, Al-Rafidain Engineering, **14**(2), 100-108.
4. Gunn, R. N., (2003). *Duplex Stainless Steels:*

Microstructure, Properties and Applications, Abington Publishing, Cambridge.
5. Jebaraja A. V., Ajaykumar L., Deepak C. R., Aditya K. V. V., (2017). *Weldability, machinability and surfacing of commercial duplex stainless steel AISI2205 for marine applications – A recent review*, Journal of Advanced Research, **8**(3), 183-199.
6. Knyazeva M., Pohl M., (2013). *Duplex Steels: Part I: Genesis, Formation, Structure*, Metallography, Microstructure, and Analysis, **2**, 113–121.
7. Rosso M., Peter I., Suani D., (2013). About heat treatment and properties of Duplex Stainless Steels, Journal of Achievements in Materials and Manufacturing Engineering, **59**(1), 26-36.
8. Tahchieva A. B., Llorca-Isern N., Cabrera J-M., (2019). *Duplex and Superduplex Stainless Steels: Microstructure and Property Evolution by Surface Modification Processes*, Metals, **9**(3), 347.
9. *The Avesta Welding Manual, Practice and products for stainless steel welding*. Available from: http://www-eng.lbl.gov/~shuman/NEXT/MATERIALS&COMPONENTS/Pressure_vessels/ss_weld_manual_avesta.pdf. Accessed: 11/04/2019.
10. Zappa S., Surian E., Svoboda H., (2013). *Effects of Welding Procedure on Corrosion Resistance and Hydrogen Embrittlement of Supermartensitic Stainless Steel Deposits*, Journal of Iron and Steel Research, International, **20**(12), 124-132.

Received: March 15, 2020 / Accepted: December 20, 2020 / Paper available online: December 25, 2020